

### DEVELOPING SPACE WEATHER MONITORING GADOLINIUM LOADED CHERENKOV WATER TANKS IN GEANT 4

Almahdi Elhamri

200164805

Academic Supervisor: Patrick Stowell

Lab partner: Sam Whitehead

Department of Physics and Astronomy

University of Sheffield

PHY31002

2024

#### Abstract

This study explores the geometry and simulation techniques employed in designing a Cherenkov water detector, which includes suspending a lead producer within a liquid moderator composed of water doped with 0.2% gadolinium sulfate. The goal is to create cost-effective and compact neutron monitors for space weather applications using Geant 4 simulations, facilitated by PyCrust. The detector operates by capturing thermal neutrons generated through spallation events when fast neutrons interact with nuclei in the lead producer. These thermal neutrons are then absorbed by gadolinium<sup>157</sup> isotope, emitting gamma rays capable of inducing Compton electrons, which in turn produce Cherenkov light cones. Computational strategies such as employing a hemispherical custom generator revealed the detector's ability to generate gamma rays, potentially leading to the production of Cherenkov light cones. This capability showed variations depending on the placement and thickness of the lead producer within the water. Furthermore, distinct behaviors were observed between cascade neutrons at energies such as 100 MeV and other slower energy sources like evaporation or thermal neutrons from alternative origins. This suggests the possibility of mitigating the detection of evaporation and thermal neutrons, thereby enhancing the detector's selectivity for specific neutron sources.

#### 1. INTRODUCTION

Earth is regularly bombarded by a substantial flux of cosmic rays originating from both solar and galactic sources, with solar activity exacerbating their incidence, particularly during events like solar flares and coronal mass ejections (CMEs) [1]. These phenomena lead to an increased influx of solar energetic particles (SEPs) ranging from high-end KeVs to 10 GeV, consisting notably of protons capable of traversing Earth's magnetic field and colliding with atmospheric particles, thereby producing extensive air showers (EAS) that reach the Earth's surface. This sudden increase in cosmic ray detection is known as ground-level enhancements (GLEs) [2]. GLE events are rare, occurring approximately once per year, and while societal ramifications are generally modest, not all potential effects are fully understood [3, 4]. In high-altitude scenarios, particularly in aviation and astronautics where human beings are most exposed, multiple studies have attempted to discern the consequences of cosmic rays on the nervous system [5, 6]. Furthermore, discussions have arisen regarding how GLE events significantly alter atmospheric electrical

properties such as conductivity, electric field strength, air–earth conduction current, and potentially the Ionospheric Potential [7]. They also pose a danger to electronic equipment, particularly in aviation, where enhanced radiation levels during GLEs can trigger single-event upsets in electronic components, potentially causing malfunctions or data corruption in critical systems [8]. Therefore, it is of scientific interest to develop techniques to detect these events.

Neutron monitors are a common ground-based form of detection for the nucleonic components of particle showers, occurring when cosmic rays collide with molecules in the upper atmosphere, causing the release of neutrons as the atmospheric molecules or atoms become unstable and decay. Various design implementations of space monitoring detectors, usually Cherenkov detectors with neutron monitoring capabilities, have been deployed across the globe, such as the Spaceship Earth neutron monitoring network and, to a lesser extent, the Super-Kamiokande neutrino detector, which has capabilities but is tailored toward neutrino detection [9, 10, 11].

However, the issue that prevails over these detectors is their costliness to construct and the difficulty in moving and operating them in certain locations due to their size and functional requirements. This paper will continue the development of a detector geometry specified in the literature "Gadolinium loaded Cherenkov detectors for neutron monitoring in high energy air showers," which details the use of a water-based moderator loaded with gadolinium in two separate tanks, each with a photomultiplier tube (PMT), stacked on either side of a lead producer for a lower-cost, smaller design [12]. The aim is to simplify the design further by removing duplicate components and testing if the detector still produces similar results. Additionally, various configurations will be explored regarding the placement and dimensions of the lead producer to gain a greater understanding of potentially more complex geometries and to develop computational methods for future use.

The remainder of this paper will cover four further sections. The first of these sections will delve into the theory, covering the physical processes inside a water Cherenkov detector. It will then progress to the computational elements of Geant 4, including selected geometries and generator designs. This will transition to a methodology discussing how each run was set up to achieve the desired plots seen in the results section. Finally, the paper will culminate in a comprehensive analysis and discussion of the simulation results obtained.

## 2. THEORY

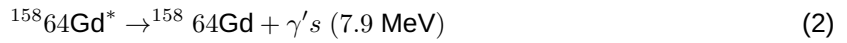
Cherenkov or Cerenkov detectors are primarily used to detect incidences of neutrino cosmic rays or charged particles from air showers, specifically looking to detect a propagating Cherenkov light cone—an observed feature where a charged particle moves faster at the speed of light in a sufficiently dense medium such as liquid water, tending to the blue end of the optical spectrum. A neutron monitor operates in a similar manner but through a spallation event, an inelastic nuclear reaction. In this process, high-energy particles collide with a stable nucleus, causing it to either decay into daughter components and emit additional neutrons or just release fragments. These secondary neutrons are slowed down to thermal speeds by both the spallation event and the moderator, making them susceptible to absorption by a dopant, which in this case is gadolinium.

Gadolinium is a particularly attractive choice as a dopant due to its two stable isotopes,  $\text{Gd}^{155}$  and  $\text{Gd}^{157}$ , both possessing notably high thermal cross-sections of  $6.1 \times 10^4$  barns and  $2.54 \times 10^5$  barns, respectively—among the highest known for any isotope.  $\text{Gd}^{157}$  allows for the capture of a thermal neutron that ends up producing a  $\gamma$ -ray cascade [13].



Here,  $n_{\text{th}}$  represents a thermal neutron, and the superscript "\*" indicates that the gadolinium nucleus is in an excited state following neutron capture.

Upon capturing a neutron, the excited gadolinium nucleus rapidly de-excites, typically through the emission of one or more  $\gamma$  rays. The total energy released in the gamma-ray cascade is approximately 7.9 MeV, corresponding to the energy difference between the excited state and the ground state of the gadolinium nucleus [14]:



These  $\gamma$ -rays travel through the water gadolinium sulfate-doped medium until Compton scattering comes into effect and Cherenkov light is produced from the release of a loosely bound electron, a process depicted in Figure 1 below [15]:

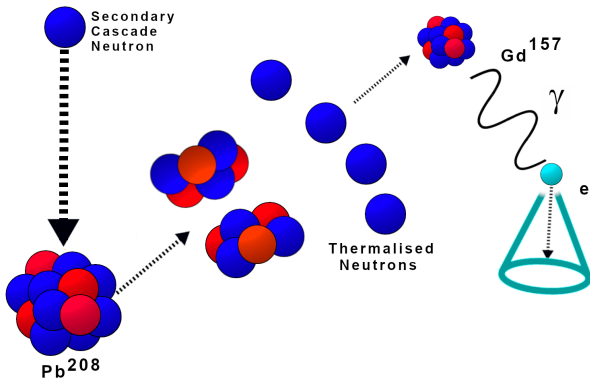


**Figure 1:** Illustration of a fast cascade neutron impacting a lead atom and creating thermal neutrons, which excite gadolinium nucleus that later de-excites and emits gamma rays. Through Compton scattering, these gamma rays produce an electron resulting in a Cherenkov cone.

If the photons are within the optical range, they should be detected by the photomultiplier tube and reach the photocathode. This excites the electrons within the photocathode, causing them to be ejected from the material and continue down the photomultiplier. The photomultiplier contains dynodes that act as multipliers; as the electrons hit the surface of the dynodes, they further excite more electrons. By the end of the photomultiplier anode, the initial signal would have been increased substantially.

The spectrum of atmospheric neutrons has specific peaks relating to different interactions. A defined peak centred at 100 MeV relates to the cascade interaction following primary cosmic ray collisions. From approximately 10 MeV to 0.1 MeV is a broad peak usually defined as the evaporation peak, and finally, the thermal range is less than 1 eV [16].

### 3. GEANT 4 SIMULATIONS

#### 3.1. Geometry

The geometry consists of only one water tank, contrasting with the study "Gadolinium loaded Cherenkov detectors for neutron monitoring in high energy air showers." The tank is a hollow cylinder constructed from Geant 4's Aluminum material, with dimensions of 40 cm in height and a radius of 16 cm. It is encased by a High-Density Polyethylene (HDPE) cylinder, providing shielding for low-energy neutrons and charged particles such as protons. Internally, the tank is filled with a cylinder of gadolinium sulfate-loaded water, with a radius of 15 cm and a height of 38 cm, centered so that the aluminum tank thickness is 1 cm. Placed within this water is a lead cube measuring 15 cm in length, 5 cm in width, and 5 cm in depth, as illustrated in Figure 2:

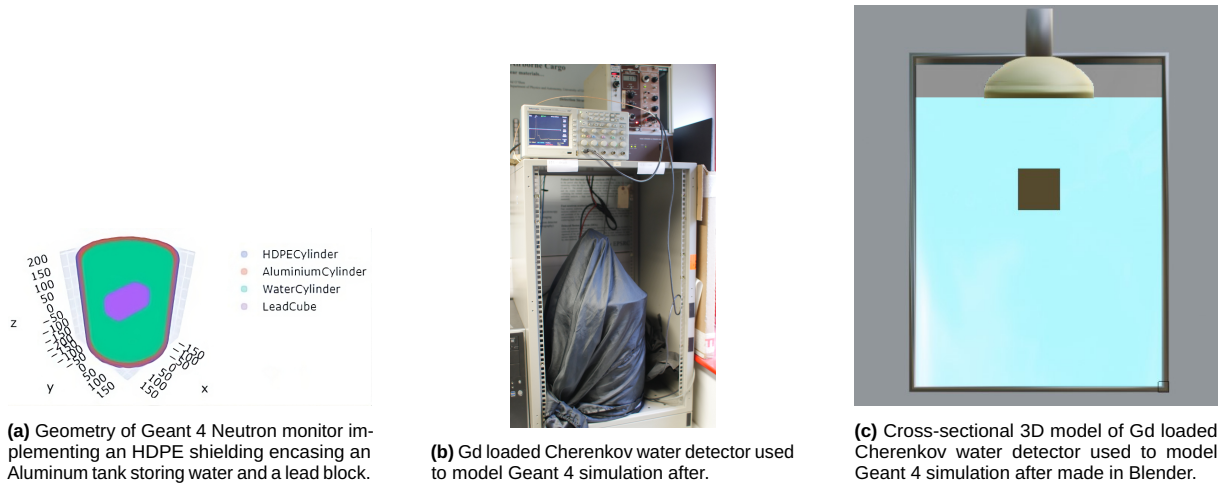


Figure 2: Detector Geometry

#### 3.2. Physics List

Geant 4, being a high-energy particle, Nuclear, and accelerator physics toolkit, is useful software for testing and validating potential design ideas for the neutron Cherenkov detector. However, there are many variations due to differences in potential applications [17]. Hence, it's important to highlight these decisions. PyCrust, a Python-written shell, was used due to its simplicity compared to Geant 4's base code C++. This choice doesn't affect the simulation; it only impacts how the code is written. The Physics list used was QGSP BERT HP, or the Quark Gluon String Model physics Bertini Cascade Model High Precision neutron model, which enables good modeling of neutron production and transport with energies less than 20 MeV. This will be particularly useful when propagating thermalized neutrons, as they possess energy below 20 MeV. HepRandom, originally a module developed for Geant4, was also used to randomize each run's seed, ensuring that each run of the simulation starts with a different sequence of random numbers, thereby introducing variability into the simulation results. Gadolinium sulfate was added to G4Water at 0.2% of the total volume, following the loading used at the Super-Kamiokande neutrino detector [18].

### **3.3. Custom Generator**

A custom generator was constructed to shoot particles at the lead target, modelled after the literature "DOME: Discrete Oriented Muon Emission in GEANT 4 Simulations," which creates a hemispherical area around the detector that fires neutrons. The aim is to replicate real-world conditions of what a neutron monitor would experience and remove the central bias that having a point source generator or even a circle would introduce [19]. The radius of the sphere was set at 2.05 meters away from the origin of the geometry to avoid potential clipping through the geometry. It was decided against implementing slight randomness to the direction of the neutrons, as for large radii, many neutrons would not interact with the lead, and the simulation would become dependent on the random number assigned for the seed. An event counter was also attached to the custom generator, recording the chronology of events. This is useful for measuring the energy deposition, as it allows for easier differentiation of interactions that don't occur simultaneously, such as photon cascades from gadolinium de-excitation versus unique events such as transfers of a neutron's kinetic energy through water, which is unlikely to be captured if it exceeds the water's cross-section.

### **3.4. Sensitive Detectors**

A sensitive detector is a part of the geometry that is sensitive to the passage of particles and provides a read-out for the events that occur within said element of the geometry. Logically, the sensitive detector geometry would be the water cylinder, comprising two different types of sensitive detectors.

Firstly, the Energy Deposit sensitive detector allows for the detection of points at which particles deposit energy in the system, either through gamma-ray emission or collision with water molecules. To make this useful in finding cases of Cherenkov light, the energy deposition detector is given an event counter, where the condition is that energy deposition must be greater than zero. Since the capture of a neutron by gadolinium results in a cascade of gamma rays, the data can be filtered for instances where multiple cases of energy deposition occur in the same event.

Additionally, a neutron tagger was added to the Energy Deposition, which works by adding another energy deposition sensitive detector to the lead. This looks for cases in which the energy deposition is greater than zero and labels the iteration as a neutron-interacted one. This condition is then applied to the energy deposition sensitive detector in the water, ensuring that only energy deposits registered in the water are from neutrons that have interacted with the lead block.

The other sensitive detector is the photon detector. This filters for only gamma rays using Geant 4's GetTrack class and its module GetPDGEncoding to find instances where a gamma ray is found in the water cylinder and collects coordinate data for it. This data can be used to calculate the probability of geometries in comparison to other variations using solid angles.

### **3.5. Solid Angle Probability**

The relative performance of the detector is determined by the summation of the solid angles of the detected gamma rays at the time of production. The equation for one gamma ray solid angle probability

is defined as:

$$\Omega = \frac{\text{Surface Area} \times \cos(\theta)}{4\pi r^2} \quad (3)$$

Here, the surface area relates to the PMT on the physical detector, which is a 9390B Series with a 130 mm optically sensitive area [20].  $r$  is the distance between the point at which the photon is detected and the surface area mimicking the photomultiplier, and  $\theta$  corresponds to the angle between the vector from the photon to the centre of the surface area and the normal from the surface area with vector (0,0,-1). However, not all gamma rays produced are in the line of sight for the surface area depending on the lead position in the simulation. Further code was written to exclude incidences where gamma rays could not propagate toward the surface area in a straight line from their position. No further code was produced for simulating Cherenkov radiation due to the complexity of the code required.

#### 4. METHODOLOGY

The computational method encompassed several variations of setups. Due to technological limitations, a neutron production count of 250,000 was decided for cases where the hemispherical generator was centred on the origin. This choice was made due to a significant number of spallations occurring from that point. Runs were tested for selected discrete energy levels of 100 MeV, 10 MeV, 5 MeV, and 1 eV to comprehensively address features within the secondary neutron spectrum. For each of these energy levels, both sensitive detectors (energy deposition and photon solid angle) were employed, and changes in the Z and Y-axis positions of the lead block were examined.

The simulations focusing on changes in the Z-axis had seven points of interest between 15 mm and -15 cm, ensuring each step was 5 cm away from the other, thus avoiding overlap from the lead block. Simulations involving changes in the Y-axis increased in steps of 2 cm from 2 to 10 cm, resulting in five data points. This limitation stemmed from the radius being only 15 cm, and concerns were raised that the length of the lead block at 15 cm might cause it to protrude inside the aluminum cylinder.

Further simulations involved examining other aspects, one of which involved analyzing energy deposition and photon angle as a function of thickness in steps of 1 cm within the range of 1 to 7 cm.

#### 5.RESULTS

After the simulations, data analysis was conducted to discern various observations. Initially, for the runs involving the energy deposition-sensitive detector, the data underwent sorting into either a frequency graph or a scatter. Due to the large amount of graphs, only the ones of interest are presented in the main body of the report, the full account is shown in the appendix.

##### 5.1 Frequency of Energy Deposition Runs

The analysis of energy deposition frequency involved aggregating the recorded energy deposition within shared event counts. Subsequently, this aggregated data was organized into bins of 2, 1, 0.5 MeV, and 0.1 eV, based on the size of the dataset. This approach aimed to either smooth out the distributions or preserve the shape of the data. Noteworthy plots from the Z displacement data can be seen in Figures 3,

4, 5, and 6, while the Y displacement isn't particularly interesting and has been left to the appendix. Each plot includes an 8 MeV vertical dash line to signify the total cascade energy released by the de-excitation of  $Gd^{157}$ .

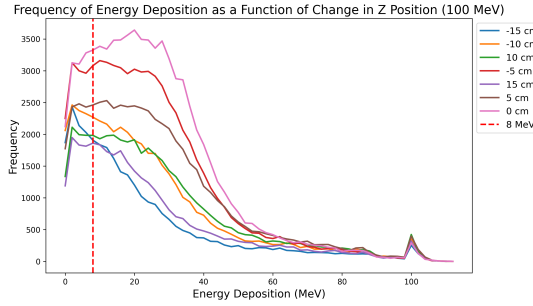


**Figure 3:** Graph illustrating simulated data obtained from 250,000 primary neutrons with an initial energy of 100 MeV. The data has been organized into bins of 2 MeV, showcasing the variation in total energy deposition as the position of the lead blocks along the Z-Axis changes from 15cm to -15cm.

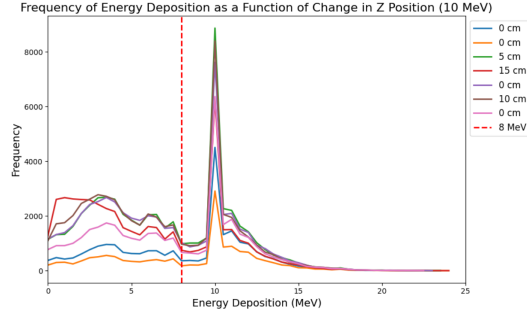


**Figure 4:** Graph illustrating simulated data obtained from 250,000 primary neutrons with an initial energy of 10 MeV. The data has been organized into bins of 1 MeV, showcasing the variation in total energy deposition as the position of the lead blocks along the Z-Axis changes from 15cm to -15cm.

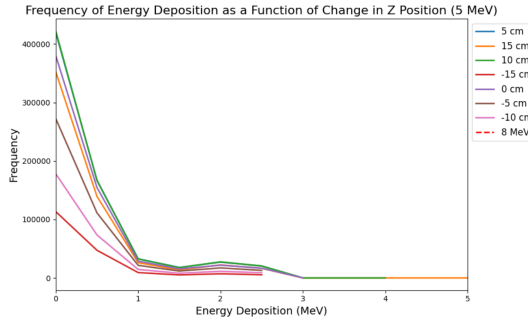


**Figure 5:** Graph illustrating simulated data obtained from 250,000 primary neutrons with an initial energy of 5 MeV. The data has been organized into bins of 0.5 MeV, showcasing the variation in total energy deposition as the position of the lead blocks along the Z-Axis changes from 15cm to -15cm.

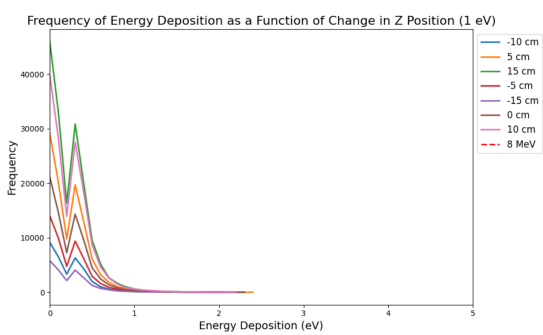


**Figure 6:** Graph illustrating simulated data obtained from 250,000 primary neutrons with an initial energy of 1 eV. The data has been organized into bins of 0.1 eV, showcasing the variation in total energy deposition as the position of the lead blocks along the Z-Axis changes from 15cm to -15cm.

From the 100 MeV frequency plot, it can be observed that there is enough energy deposition beyond the 8 MeV mark to suggest a significant amount of thermal neutron absorption by the gadolinium present in the water. In this configuration, it is reasonable to believe that in the case of GLEs, the neutron monitor would detect space weather events. One surprising result is that the position -5 cm is much more favored and produces a much greater yield of energy deposition than its positive counterpart at 5 cm, with the frequency being highest past the 8 MeV line at approximately 500. This may be due to the hemispherical generator being centered at the origin. The other negative-positive pairs, such as -10, 10, -15, and 5, perform fairly similarly. Beyond just the 100 MeV runs, the 5 MeV and 1 eV runs show no cases of Gd neutron absorption and likely only observe the result of water absorption of the neutrons. For the 10 MeV run, there is a noticeable dip after the 8 MeV dashed line, but there are still enough cases to suggest some absorption of neutrons from the gadolinium. For both the 100 MeV and 10 MeV plots, there is a strong peak centered around the primary particle kinetic energy, though it's unknown why that is occurring, as it's unlikely to be absorption of a single particle with 100 MeV if it has interacted with the lead block due to the requirement from the neutron tagger.

## 5.2 Energy Deposition Runs: Z Displacement

For the scatter graphs, the total energy deposition of each point was recorded and plotted in a displacement/dimension graph against total energy deposition. For the Z displacement, the 100 MeV run favors a peak displacement of -1.06 cm according to the line fit, which generally fits with what is seen in the frequency graph. For the 10, 5 MeV, and 1 eV runs, the peak tends to a higher displacement, as seen in Figures 7, 8, 9, and 10.

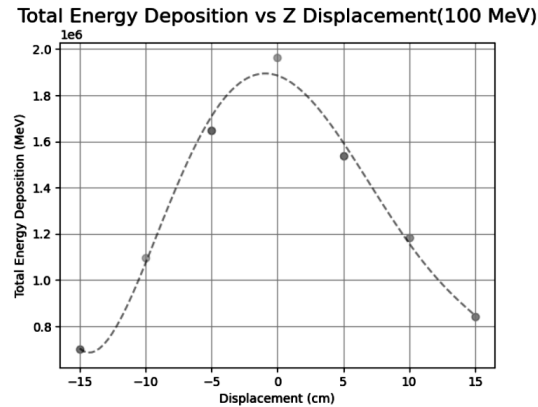


**Figure 7:** Graph showing simulated total energy deposition versus the lead block's Z-axis position (from 15 cm to -15 cm in 5 cm increments) for 100 MeV neutrons. The peak energy deposition of  $1.96 \times 10^6$  MeV occurs at 0 cm, with a line skewness of 0.18 and a peak displacement of -1.06 cm.

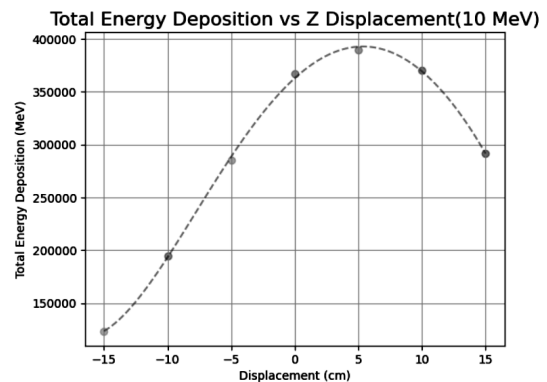


**Figure 8:** Graph showing simulated total energy deposition versus the lead block's Z-axis position (from 15 cm to -15 cm in 5 cm increments) for 10 MeV neutrons. The peak energy deposition of  $3.89 \times 10^5$  MeV occurs at 5 cm, with a line skewness of -0.61 and a peak displacement of 5.3 cm.

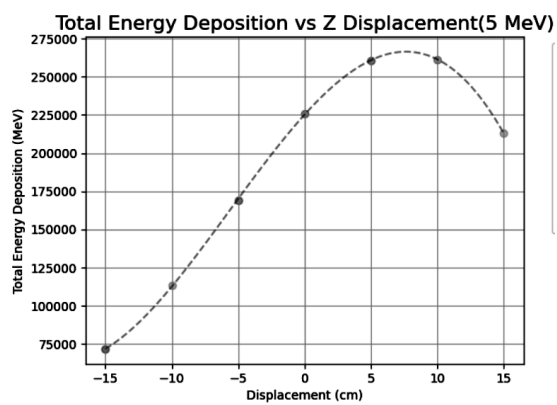


**Figure 9:** Graph showing simulated total energy deposition versus the lead block's Z-axis position (from 15 cm to -15 cm in 5 cm increments) for 5 MeV neutrons. Peak energy depositions of  $2.61 \times 10^5$  MeV occur at both 5 and 10 cm, with a line skewness of -0.52 and a peak displacement of 7.73 cm.

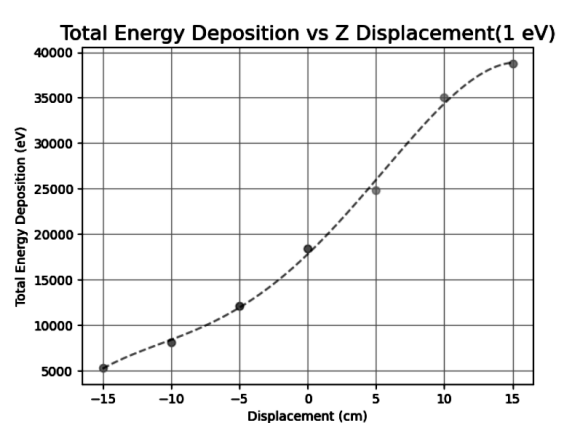


**Figure 10:** Graph showing simulated total energy deposition versus the lead block's Z-axis position (from 15 cm to -15 cm in 5 cm increments) for 1 eV neutrons. The peak energy deposition of  $3.87 \times 10^4$  MeV occurs at 15 cm, with a line skewness of 0.29.

## 5.3 Energy Deposition Runs: Y Displacement

The Y displacement plots for 10 MeV and lower show steady gradients from 2 cm to 10 cm without any deviations. However, for the 100 MeV plots, an upturn was observed at 10 cm.

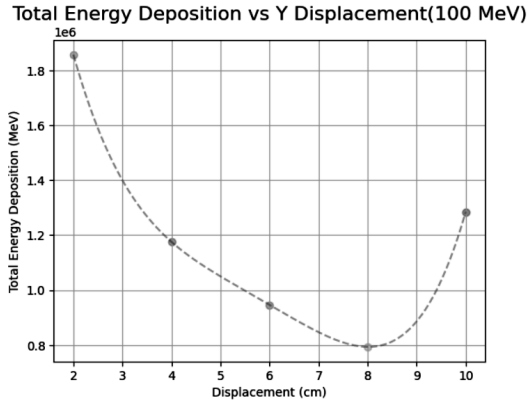


**Figure 11:** Graph showing simulated total energy deposition versus the lead block's Y-axis position (from 2 cm to 10 cm in 2 cm increments) for 100 MeV neutrons. The peak energy deposition of  $1.86 \times 10^6$  MeV occurs at 2 cm.

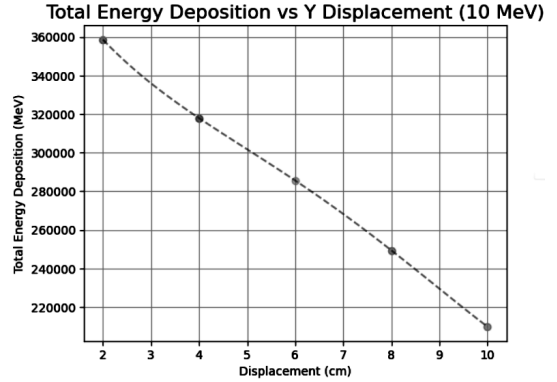


**Figure 12:** Graph showing simulated total energy deposition versus the lead block's Y-axis position (from 2 cm to 10 cm in 2 cm increments) for 10 MeV neutrons. The peak energy deposition of  $3.59 \times 10^5$  MeV occurs at 2 cm.

#### 5.4 Solid Angle Probabilities

Solid angle probability analysis employs removing blocked gamma rays from the total summation, this is represented by the arrow vector which shows the previous total amount before the exclusion. Only 100 MeV runs are shown in the main body as the lower energies lack any unique distributions. For Figure 14, the 8 cm runs didn't compute; this is the case for all Y displacement solid angle runs.

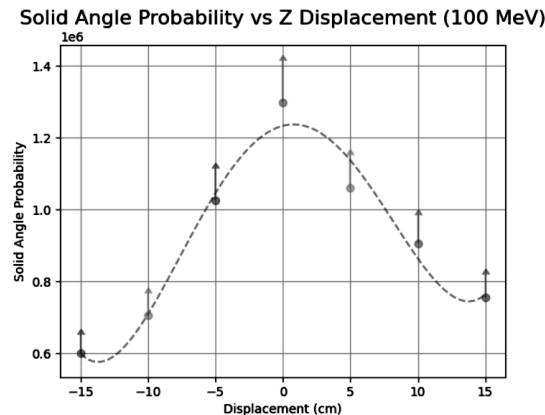


**Figure 13:** Graph showing the summated solid angles of simulated gamma-ray versus the lead block's Z-axis position (from -15 cm to 15 cm in 5 cm increments) for 100 MeV neutrons. Vector arrows indicate the blocked gamma rays by the lead block to the line of sight to the mock PMT.

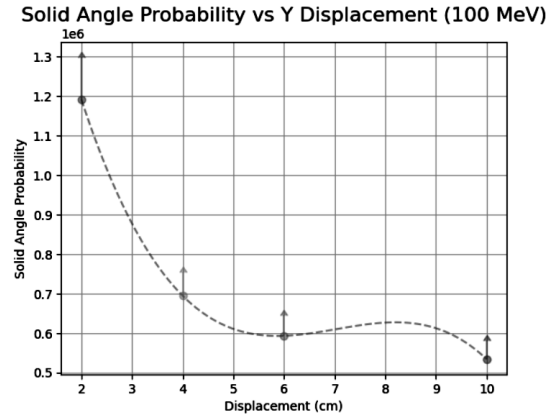


**Figure 14:** Graph showing the summated solid angles of simulated gamma-ray versus the lead block's Y-axis position (from 2 cm to 10 cm in 2 cm increments) for 100 MeV neutrons. Vector arrows indicate the blocked gamma rays by the lead block to the line of sight to the mock PMT.

Both graphs show peaks at central positions of 0 cm and 2 cm, respectively, and there is an increasing number of blocked gamma rays at these positions. However, this may be an instance of proportionality with the increased number of gamma rays produced. For the Z-axis displacement, there is a stronger bias toward the position near the top of the detector in contrast to the energy deposition runs.

#### 5.5 Thickness Runs

The thickness data analysis involved the same methods implemented for the energy deposition and solid angle probability plots. The 7 cm run for the solid angle probability was not able to be computed due

to time and technological constraints. As seen in Figures 15 and 16, there is a predictable slope that gradually increases. For the total energy deposition, there is a relatively small increase from  $0.96 \times 10^8$  MeV at 1 cm to  $1.01 \times 10^8$  MeV, which results in a predictable increase of  $2 \times 10^6$ . The solid probability graph increases steeply with a 134% increase over 6 cm, while the block gammas represented by the arrow vectors also increase throughout the plot. They are all consistently 9% of the unobstructed gammas' solid angles, with the difference between 1 cm and 6 cm only being 0.05%.

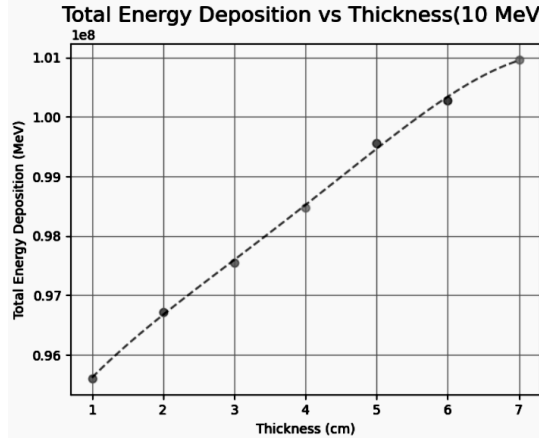


**Figure 15:** Graph of simulated data of total energy deposition against the change of the lead thickness along the Z-Axis from 1 cm to 7 cm.

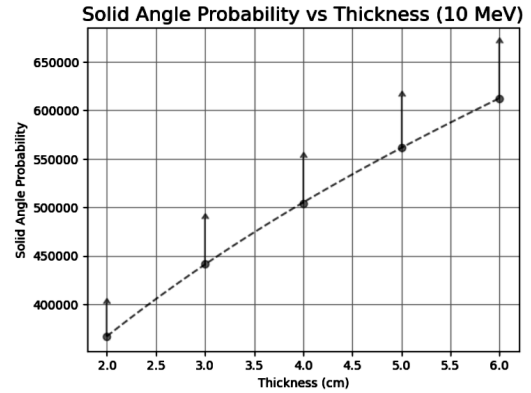


**Figure 16:** Graph of simulated data of summated solid angle probabilities of the produced gamma rays against the change of the lead thickness along the Z-Axis from 1 cm to 6 cm. Arrow vectors indicate the blocked gamma rays by the lead producer.

## 6. DISCUSSION & CONCLUSION

The results suggest that incorporating one PMT and the lead producer inside the tank represents a natural evolution of the detector geometry outlined in the literature "Gadolinium loaded Cherenkov detectors for neutron monitoring in high-energy air showers," aiming for simplification. Additionally, the findings generally align with intuitive expectations, showing a stronger bias towards the upper half of the detector at lower energies. However, it's surprising that the 100 MeV setup performs better when the lead is positioned lower in the water, especially considering that these energies are beyond the focus of the hemispherical custom generator. This preference might be attributed to the need for more neutron moderation before reaching the lead producer.

As mentioned in section 5.1, the geometry appears responsive to fast cascade neutrons of 100 MeV, performing optimally at Z=0 cm. This could stem from the inherent bias of the hemispherical custom generator but includes abnormalities like the small peak around 100 MeV, which is also observed in the 10 MeV runs with a 10 MeV peak, but not in the 5 MeV or 1 eV runs. This recurring feature suggests scenarios where multiple interactions are recorded as the same event count due to simultaneous interactions in Geant 4 which are not necessarily linked. Scrutinizing the raw data confirms this, showing different instances of energy deposition occurring at varying distances from each other. This feature will need adjustment in future studies. Additionally, the highest combined instance of two close energy deposits was approximately 19 MeV, with individual values of 9 MeV and 10 MeV likely being gamma rays produced after a gadolinium absorption event, which is much lower than the incident energy but with a high likelihood of generating more Compton electrons due to the excess energies they carry.

Positioning the lead block lower in the detector appears effective in limiting energy deposition from non-cascade neutrons. However, the extent of this effectiveness remains uncertain due to the bias of the hemispherical custom generator. It may necessitate reevaluation, perhaps by centering the hemisphere below the detector to reduce bias towards any specific area. This idea was contemplated during the simulation process.

An unexpected finding was the increase in energy deposition in the Y axis for 100 MeV between 8 cm and 10 cm, suggesting that placing some form of producer closer to the tank wall in a more intricate geometry setup might enhance the yield of thermal neutrons from cascade neutrons. Evaporation and slower neutrons do not seem affected by this choice in geometry. A potential future geometry could involve exploring a thin lead lining around the water while containing a suspended lead producer in the middle, compared to the current setup, to ascertain which configuration utilizes the same mass for greater efficiency. Additionally, the analysis of solid angle probability indicates that placing the lead in the tank does not notably diminish the chances of observing Cherenkov light concerning the position of the lead producer through blocking the line of sight.

This study suggests that the geometry setup with a lead producer suspended or incorporated within the liquid moderator could be a viable approach for more cost-effective and compact space weather monitors. However, further simulations are necessary with reduced bias or an even more realistic custom generator that accounts for neutrons reflected off the surface around the detector. Implementing optical analysis to simulate Cherenkov light creation and a more focused examination of shielding should also be considered, as these aspects were beyond the scope of this paper.

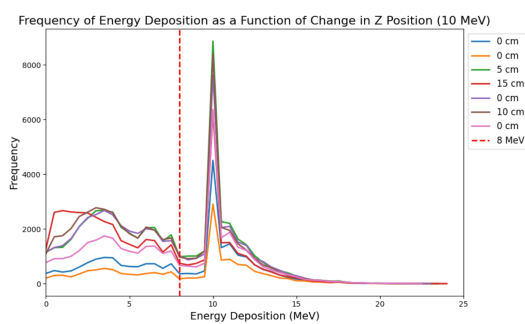
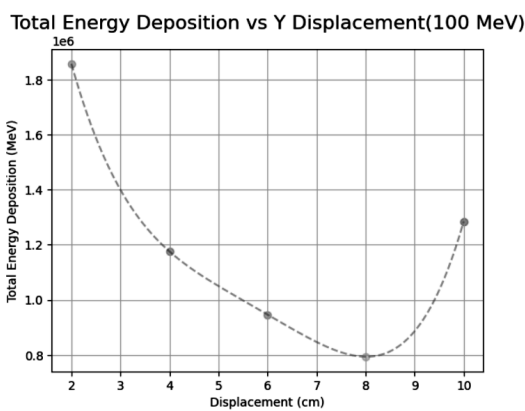
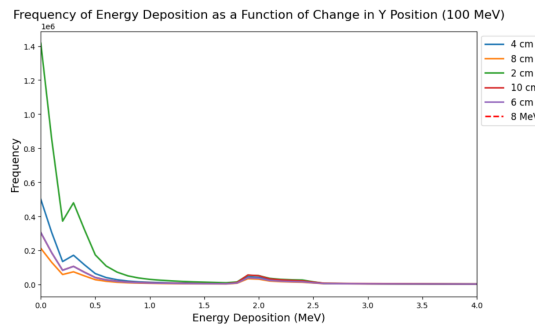
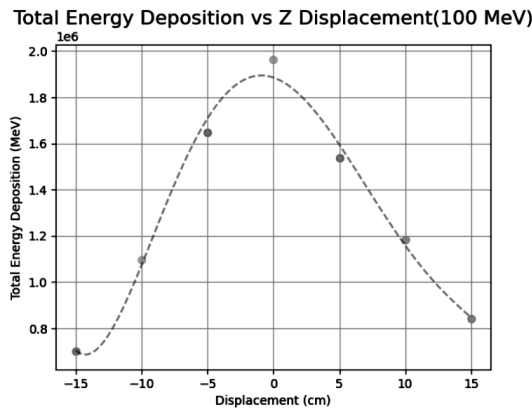
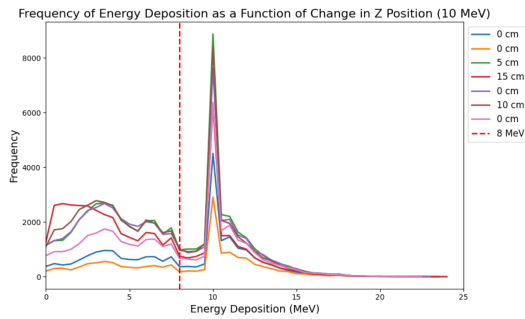
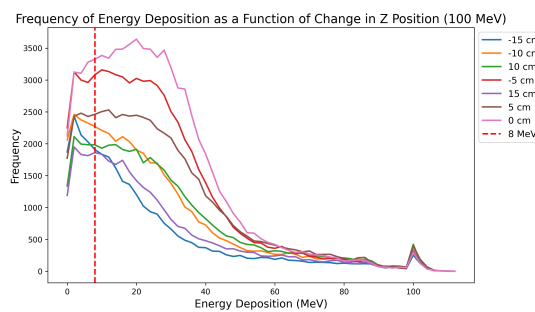
## REFERENCES

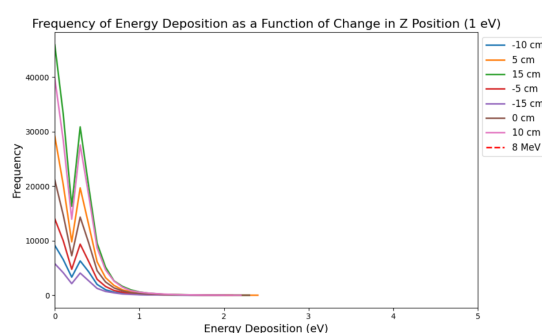
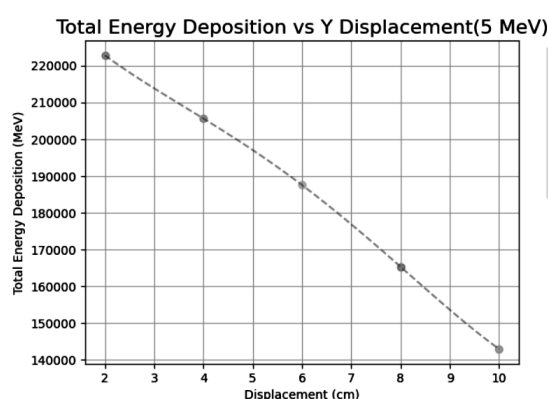
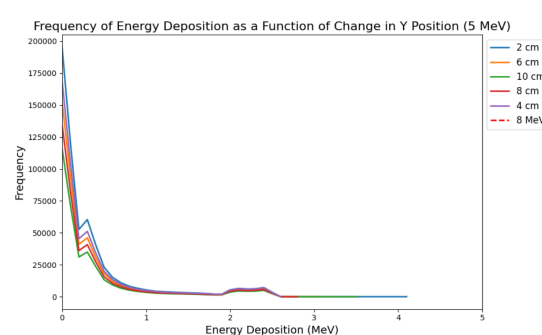
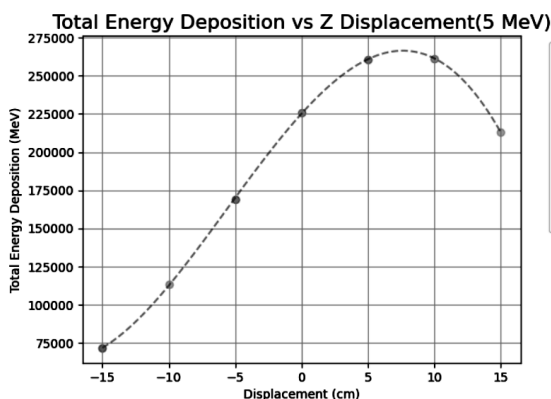
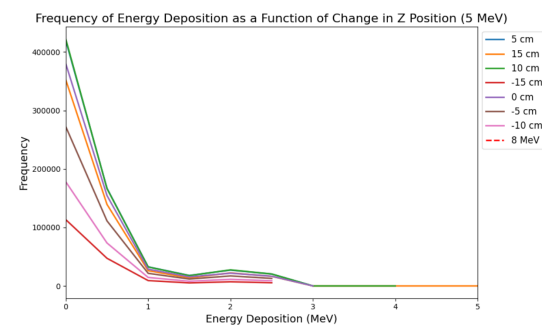
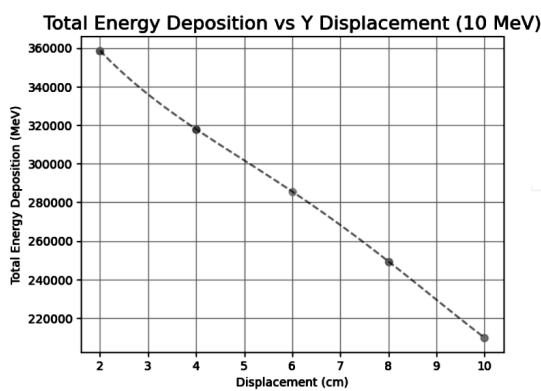
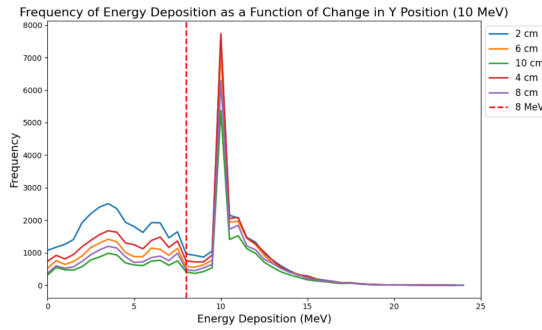
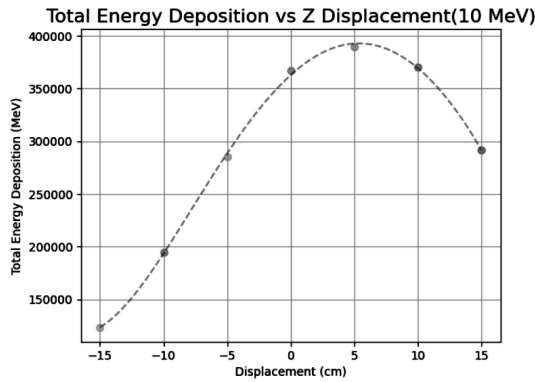
- [1] Donald V. Reames. "The Two Sources of Solar Energetic Particles". In: *Space Science Reviews* 175.1 (June 2013), pp. 53–92. ISSN: 1572-9672. DOI: [10.1007/s11214-013-9958-9](https://doi.org/10.1007/s11214-013-9958-9). URL: <https://doi.org/10.1007/s11214-013-9958-9>.
- [2] Stepan Poluianov, Ilya Usoskin, Alexander Mishev, Don Smart, and Margaret Shea. "Revisited definition of GLE". In: Sissa Medialab Srl, 2017. DOI: [10.22323/1.301.0125](https://doi.org/10.22323/1.301.0125).
- [3] Rami Vainio, Osku Raukunen, Allan J. Tylka, William F. Dietrich, and Alexandr Afanasiev. "Why is solar cycle 24 an inefficient producer of high-energy particle events?" In: *Astronomy and Astrophysics* 604 (Aug. 2017). ISSN: 14320746. DOI: [10.1051/0004-6361/201730547](https://doi.org/10.1051/0004-6361/201730547).
- [4] Alexander Mishev and Piers Jiggens. "Preface to measurement, specification and forecasting of the Solar Energetic Particle (SEP) environment and Ground Level Enhancements (GLEs)". In: *Journal of Space Weather and Space Climate* 9 (2019). ISSN: 21157251. DOI: [10.1051/swsc/2019003](https://doi.org/10.1051/swsc/2019003).
- [5] Moe Fujita, Tatsuhiko Sato, Susumu Saito, and Yosuke Yamashiki. "Probabilistic risk assessment of solar particle events considering the cost of countermeasures to reduce the aviation radiation dose". In: *Scientific Reports* 11 (1 Dec. 2021). ISSN: 20452322. DOI: [10.1038/s41598-021-95235-9](https://doi.org/10.1038/s41598-021-95235-9).
- [6] Vipan K. Parihar et al. "Cosmic radiation exposure and persistent cognitive dysfunction". In: *Scientific Reports* 6 (Oct. 2016). ISSN: 20452322. DOI: [10.1038/srep34774](https://doi.org/10.1038/srep34774).
- [7] Sotirios A. Mallios, Athanasios Papaioannou, Konstantin Herbst, Georgios Papangelis, and George Hloupis. "Study of the Ground Level Enhancements effect on atmospheric electric properties and mineral dust particle charging". In: *Journal of Atmo-*

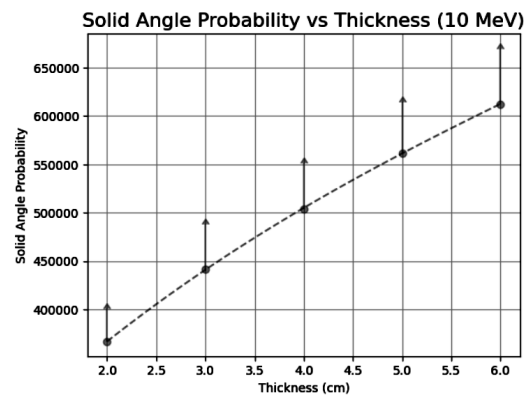
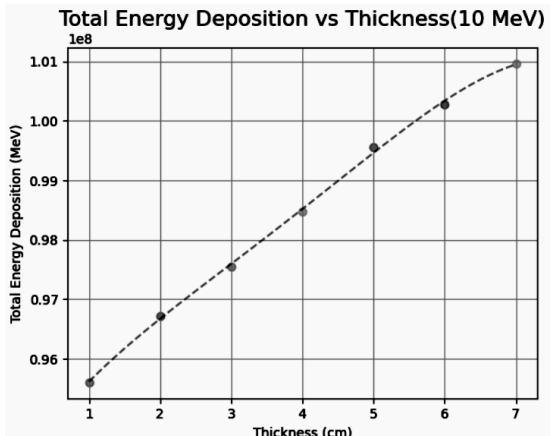
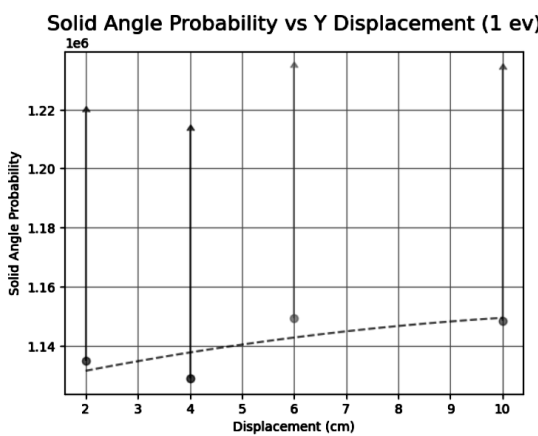
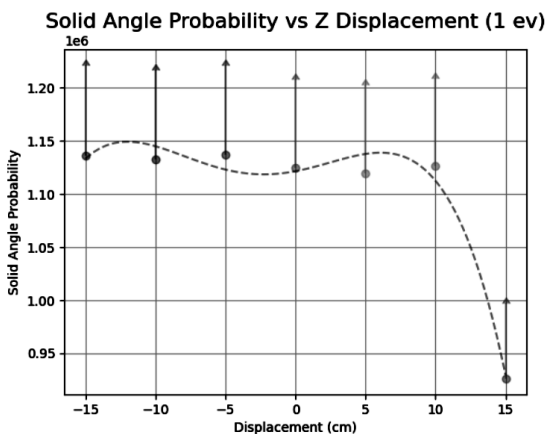
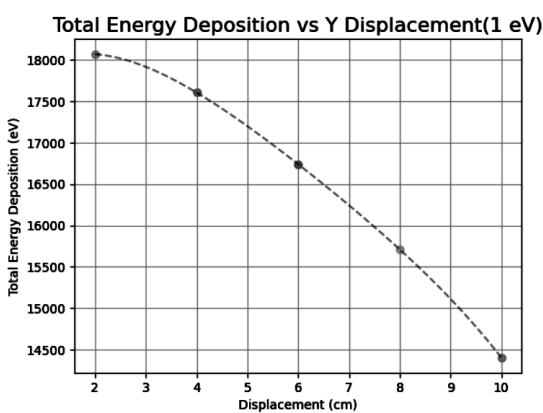
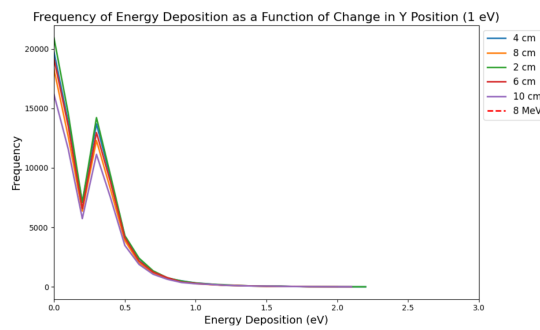
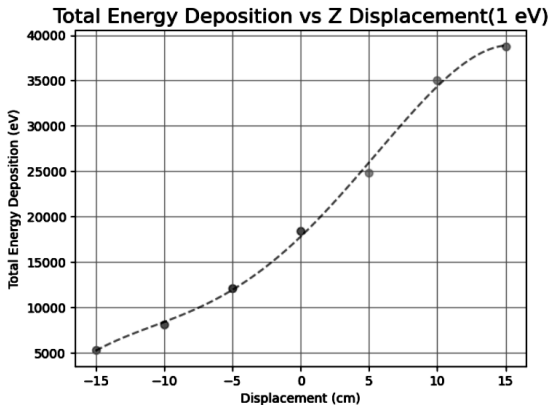
- spheric and Solar-Terrestrial Physics* 233-234 (July 2022). ISSN: 13646826. DOI: [10.1016/j.jastp.2022.105871](https://doi.org/10.1016/j.jastp.2022.105871).
- [8] Guillaume Hubert, Sébastien Aubry, and Juan Antonio Clemente. "Impact of ground-level enhancement (GLE) solar events on soft error rate for avionics". In: *IEEE Transactions on Aerospace and Electronic Systems* 56 (5 Oct. 2020), pp. 3674–3984. ISSN: 15579603. DOI: [10.1109/TAES.2020.2977792](https://doi.org/10.1109/TAES.2020.2977792).
- [9] Paul Evenson. *Spaceship Earth-An Optimized Network of Neutron Monitors*. 1995. URL: <https://www.researchgate.net/publication/234316437>.
- [10] H. Watanabe et al. "First study of neutron tagging with a water Cherenkov detector". In: *Astroparticle Physics* 31 (4 May 2009), pp. 320–328. ISSN: 09276505. DOI: [10.1016/j.astropartphys.2009.03.002](https://doi.org/10.1016/j.astropartphys.2009.03.002).
- [11] Iván Sidelnik et al. "Neutron detection capabilities of Water Cherenkov Detectors". In: *Nuclear Instruments and Methods in Physics Research, Section A: Accelerators, Spectrometers, Detectors and Associated Equipment* 952 (Feb. 2020). ISSN: 01689002. DOI: [10.1016/j.nima.2019.03.017](https://doi.org/10.1016/j.nima.2019.03.017).
- [12] P. Stowell, S. Fargher, L.F. Thompson, A.M. Brown, and P.M. Chadwick. "Gadolinium loaded Cherenkov detectors for neutron monitoring in high energy air showers". In: *Journal of Instrumentation* 17 (2 Feb. 2022). ISSN: 17480221. DOI: [10.1088/1748-0221/17/02/T02005](https://doi.org/10.1088/1748-0221/17/02/T02005).
- [13] Atsushi Kimura et al. "Neutron capture and total cross-section measurements of  $^{155}\text{Gd}$  and  $^{157}\text{Gd}$  at ANNRI in J-PARC". In: *EPJ Web of Conferences* 239 (2020), p. 01012. DOI: [10.1051/epjconf/202023901012](https://doi.org/10.1051/epjconf/202023901012).
- [14] Tomoyuki Tanaka et al. "Gamma-ray spectra from thermal neutron capture on gadolinium-155 and natural gadolinium". In: *Progress of Theoretical and Experimental Physics* 2020 (4 Apr. 2020). ISSN: 20503911. DOI: [10.1093/ptep/ptaa015](https://doi.org/10.1093/ptep/ptaa015).
- [15] Kosuke Tanabe et al. "Development of a water Cherenkov neutron detector for the active rotation method and demonstration of nuclear material detection". In: *Journal of Nuclear Science and Technology* 60 (7 2023), pp. 769–781. ISSN: 00223131. DOI: [10.1080/00223131.2022.2143449](https://doi.org/10.1080/00223131.2022.2143449).
- [16] M. S. Gordon, P. Goldhagen, K. P. Rodbell, T. H. Zabel, H. H.K. Tang, J. M. Clem, and P. Bailey. "Measurement of the flux and energy spectrum of cosmic-ray induced neutrons on the ground". In: vol. 51. Dec. 2004, pp. 3427–3434. DOI: [10.1109/TNS.2004.839134](https://doi.org/10.1109/TNS.2004.839134).
- [17] S. Agostinelli et al. "Geant4—a simulation toolkit". In: *Nuclear Instruments and Methods in Physics Research Section A: Accelerators, Spectrometers, Detectors and Associated Equipment* 506.3 (2003), pp. 250–303. ISSN: 0168-9002. DOI: [https://doi.org/10.1016/S0168-9002\(03\)01368-8](https://doi.org/10.1016/S0168-9002(03)01368-8). URL: <https://www.sciencedirect.com/science/article/pii/S0168900203013688>.
- [18] K. Abe et al. "First gadolinium loading to Super-Kamiokande". In: *Nuclear Instruments and Methods in Physics Research, Section A: Accelerators, Spectrometers, Detectors and Associated Equipment* 1027 (Mar. 2022). ISSN: 01689002. DOI: [10.1016/j.nima.2021.166248](https://doi.org/10.1016/j.nima.2021.166248).
- [19] Jacques E Marteau, Antonio Ereditato, Ahmet İlker Topuz, Madis Kiisk, and Andrea Giannanco. "DOME: Discrete Oriented Muon Emission in GEANT4 Simulations". In: (2022). DOI: [10.3390/instruments](https://doi.org/10.3390/instruments). URL: <https://doi.org/10.3390/instruments>.
- [20] ET Enterprises Limited. "130 mm (5") photomultiplier 9390B series data sheet". In: (Feb. 2014). URL: <https://et-enterprises.com/products/photomultipliers/product/p9390b-series>.

# APPENDIX

## APPENDIX A: DATA GRAPHS







## Appendix B: Computational code for simulation

---

```
1 from Geant4 import *
2 import PyCRUST as pc
3 import numpy as np
4 import nbformat
5 import math
6 from nbconvert import PythonExporter
7 import time
8 seed = int(time.time())
9 #G4Random.setTheSeed(seed)
10 from IPython.display import Image
11 physics_list = QGSP_BERT_HP()
12 gRunManager.SetUserInitialization(physics_list)
13 generator = pc.generator.simple_generator.simple_generator()
14 gRunManager.SetUserAction(generator)
15 #HepRandom.setTheEngine(rand_engine)
16 HepRandom.setTheSeed(seed)
17
18 # Tell geant4 to use a simplistic generator for now.
19 generator = pc.generator.simple_generator.simple_generator()
20 gRunManager.SetUserAction(generator)
21
22 print( pc.core.db["MATERIAL"]["Water"] )
23
24 nistManager = G4NistManager.Instance()
25
26 # Define water
27 water = nistManager.FindOrBuildMaterial("G4_WATER")
28
29 # Define gadolinium
30 gd = G4Element("Gadolinium", "Gd", 64, 157.25*g/mole)
31
32 # Define sulfur
33 s = G4Element("Sulfur", "S", 16, 32.065*g/mole)
34
35 # Define oxygen
36 o = G4Element("Oxygen", "O", 8, 16.00*g/mole)
37
38 # Define gadolinium sulfate heptahydrate
39 gadoliniumSulfate = G4Material("GadoliniumSulfate", 3.8*g/cm3, 3)
40 gadoliniumSulfate.AddElement(gd, 0.572) # Mass fraction of gadolinium in gadolinium sulfate
41 gadoliniumSulfate.AddElement(s, 0.137) # Mass fraction of sulfur in gadolinium sulfate
```

```

42 gadoliniumSulfate.AddElement(o, 0.291) # Mass fraction of oxygen in gadolinium sulfate
43
44 # Define mixture
45 density = 0.988 * water.GetDensity() + 0.002 * gadoliniumSulfate.GetDensity()
46 mixture = G4Material("WaterLoadedWithGdSulfate", density, 2)
47 mixture.AddMaterial(water, 0.988)
48 mixture.AddMaterial(gadoliniumSulfate, 0.002)
49
50 number0fEvents=0
51 eventcount = 0
52 datadictgen = {}
53 datadictgen["x"] = []
54 #decreteprobs
55
56 class custom_generator(G4VUserPrimaryGeneratorAction):
57     "My Custom Generator Action"
58
59     def __init__(self):
60         G4VUserPrimaryGeneratorAction.__init__(self)
61         particle_table = G4ParticleTable.GetParticleTable()
62         particle = particle_table.FindParticle(G4String("neutron"))
63
64         self.particleGun = G4ParticleGun()
65         self.particleGun.SetParticleEnergy(100*MeV)
66         #self.particleGun.SetParticleMomentumDirection(G4ThreeVector(0, 0, -1))
67         self.particleGun.SetParticleDefinition(particle)
68
69     def GeneratePrimaries(self, event):
70         global number0fEvents
71         number0fEvents += 1
72         if number0fEvents % 1000 == 0:
73             print(number0fEvents)
74
75         # Set the particle position within a hollow sphere
76         radius = 205.0*cm
77         rand1 = G4UniformRand()
78         rand2 = G4UniformRand()
79         latitude = math.acos(2 * rand1 - 1)
80         longitude = 2 * 3.14159265359 * rand2
81
82         # Coordinates on sphere
83         x0 = radius * math.cos(latitude) * math.sin(longitude)

```

```

84     y0 = radius * abs(math.sin(latitude))
85     z0 = radius * math.cos(latitude) * math.cos(longitude)
86     rotated_y = y0 * math.cos(math.pi/2) - z0 * math.sin(math.pi/2)
87     rotated_z = y0 * math.sin(math.pi/2) + z0 * math.cos(math.pi/2)
88     y0 = rotated_y
89     z0 = rotated_z
90
91
92     self.particleGun.SetParticlePosition(G4ThreeVector(x0, y0, z0))
93
94     # Aimed at origin
95     x1 = 0
96     y1 = 0
97     z1 = 0
98     mx = x1 - x0
99     my = y1 - y0
100    mz = z1 - z0
101    mn = math.sqrt(pow(mx, 2) + pow(my, 2) + pow(mz, 2))
102    mx = mx / mn
103    my = my / mn
104    mz = mz / mn
105    self.particleGun.SetParticleMomentumDirection(G4ThreeVector(mx, my, mz))
106
107    # Set the particle time
108    self.particleGun.SetParticleTime(0)
109
110    # Generate the primary vertex
111    self.particleGun.GeneratePrimaryVertex(event)
112
113    global neutron_interacted
114    neutron_interacted = False
115
116    global eventcount
117    eventcount += 1
118
119 # Create an instance of the custom generator
120 generator = custom_generator()
121
122
123 # Set the custom generator as the user action for the run manager
124 gRunManager.SetUserAction(generator)
125

```

```

126
127 # Geometry
128
129 # We define our tank and add it to the database for record keeping
130 #Lead block placement in cm
131 z=20-5*4
132 Lead_Place= [0,0,z]
133 tank_wall = 10*mm
134 tank_height = 40*cm
135 tank_radius = 15*cm
136 HDPE_Thickness= 1*cm
137 Lead_Height= 15*cm
138 Lead_Width= 5*cm
139 Lead_Depth= 5*cm
140 geometry = [
141     {
142         "type": "GEO",
143         "index": "HDPECylinder",
144         "solid": "G4Tubs",
145         "pRMin": 0,
146         "pRMax": tank_radius + tank_wall + HDPE_Thickness,
147         "pDz": tank_height/2,
148         "pSPhi": 0,
149         "pDPhi": twopi,
150         "material": "G4_POLYETHYLENE",
151         "position": [0.0,0.0,0.0],
152         "rotation": [0,0.0,0.0],
153         "mother": "world"
154     },
155     {
156         "type": "GEO",
157         "index": "AluminiumCylinder",
158         "solid": "G4Tubs",
159         "pRMin": 0,
160         "pRMax": tank_radius + tank_wall,
161         "pDz": tank_height/2,
162         "pSPhi": 0,
163         "pDPhi": twopi,
164         "material": "G4_Al",
165         "position": [0.0,0.0,0.0],
166         "rotation": [0.0,0.0,0.0],
167         "mother": "HDPECylinder"

```

```

168     },
169     {
170         "type": "GEO",
171         "index": "WaterCylinder",
172         "solid": "G4Tubs",
173         "pRMin": 0,
174         "pRMax": tank_radius,
175         "pDz": tank_height/2-tank_wall,
176         "pSPhi": 0,
177         "pDPhi": twopi,
178         "material": "WaterLoadedWithGdSulfate",
179         "position": [0.0,0.0,0.0],
180         "rotation": [0.0,0.0,0.0],
181         "mother": "AluminiumCylinder"
182     },
183     {
184         "type": "GEO",
185         "index": "LeadCube",
186         "solid": "G4Box",
187         "pX": Lead_Height/2,
188         "pY": Lead_Width/2,
189         "pZ": Lead_Depth/2,
190         "material": "G4_Pb",
191         "position": [Lead_Place[0]*cm, Lead_Place[1]*cm, Lead_Place[2]*cm ],
192         "rotation": [0.0,0.0,0.0],
193         "mother": "WaterCylinder"
194     }
195 ]
196 ]
197 pc.core.db.add(geometry)
198
199 # Make the builder object
200 physical_geometry = pc.geometry.dictionary_construction.dictionary_construction()
201
202 # Then we ask the dictionary builder to build the world and add our objects
203 physical_geometry.create_world( side=100*mm, material="G4_AIR" )
204 physical_geometry.build_geo_from_database()
205
206 # We need to tell GEANT4 this is the world to use
207 gRunManager.SetUserInitialization(physical_geometry)
208
209 # Set up sensitive detectors

```

```

210 sd2 = energy_deposit_detector("water")
211 physical_geometry.hierarchy["WaterCylinder"]["logical"].SetSensitiveDetector(sd2)
212 sd3 = neutron_tagger("lead ")
213 physical_geometry.hierarchy["LeadCube"]["logical"].SetSensitiveDetector(sd3)
214
215 # Run the simulation
216 gRunManager.Initialize()
217 gRunManager.BeamOn(250000)
218
219 import pandas as pd
220 import time
221 import os
222 import csv
223 from pathlib import Path
224 df = pd.DataFrame(data=my_dataset)
225 df3 = pd.DataFrame(data=dataset)
226
227 sensitive_detectors = {
228     sd2: "energy_deposit_detector_water"
229 }
230 active_sd = None
231 for sd, sd_name in sensitive_detectors.items():
232     if sd:
233         active_sd = sd_name
234         break
235
236 # Construct output filename
237 if active_sd:
238     output_path=f'position_{Lead_Place[0]}_{Lead_Place[1]}_{Lead_Place[2]}_size_{Lead_Height}_{Lead_Width}_{Lead_Depth}_mother_{geometry[-1]["mother"]}_detector_{active_sd}_dataf.csv'
239     df.to_csv(output_path, mode='a', header=not os.path.exists(output_path))
240     df3.to_csv(output_path, mode='a', header=not os.path.exists(output_path))

```

---

**Listing 1:** Python Code